

16<sup>th</sup> November 2017

**Response of concrete cast in permeable moulds to severe heating**

O Richards MEng (hons)

Researcher, University of Bath, Bath, BA2 7AY

Ieuan Rickard MEng (hons)

PhD Candidate, School of Engineering, University of Edinburgh, Edinburgh, EH9 3JG

Dr J Orr MEng(hons) PhD CEng MStructE FHEA

University Lecturer in Concrete Structures, University of Cambridge, Cambridge, CB2 1PZ

Professor L Bisby BEng MSc(Eng) PhD PEng CEng FStructE FIFireE FIESIS

School of Engineering, University of Edinburgh, Edinburgh, EH9 3JG

12 **Abstract**

13 This paper evaluates the effect that a permeable mould, such as would be used to  
14 create fabric-formed concrete, may have on the heat-induced explosive spalling  
15 performance of cast concrete, using a novel experimental fire testing method and  
16 supported by scanning electron microscopy. Recent research suggests that a  
17 concrete cast using fabric formwork will gain durability enhancements at the cast  
18 surface that may negatively affect pore-pressure expulsion during severe heating. Six  
19 concrete samples were cast using high strength concrete including silica fume and  
20 tested using the University of Edinburgh's Heat-Transfer Rate Inducing System (H-  
21 TRIS), receiving thermal loading on one surface. Three samples were cast in  
22 permeable moulds, formed using a Huesker HaTe PES 70/70 single layer woven  
23 geotextile with a characteristic opening size ( $O_{90}$ ) of  $0.1 \times 10^{-3} \text{m}$ . Three samples were  
24 cast in conventional impermeable timber moulds. The tests showed no conclusive  
25 evidence of differences in thermal profile or differential thermal deflections between  
26 the two casting methods; no occurrences of heat-induced explosive spalling were  
27 observed for either casting method. However, scanning electron microscopy  
28 undertaken on additional samples showed that the test face of samples cast in  
29 permeable moulds were over four times less porous compared to their impermeably  
30 cast equivalents. This could increase the risk of spalling of samples, particularly in  
31 cases where pore-pressure spalling dominates the material response. However,  
32 additional fire testing using H-TRIS is needed under a range of heating and loading  
33 conditions, before definitive conclusions on the spalling propensity of fabric-formed  
34 concrete can be made.

35

## 36 **1 Introduction**

37 Detailed structural optimisation of concrete structures can yield material savings in  
38 the order of 40% (Orr et al., 2011). Such savings can be achieved, for example, by  
39 using flexible, permeable, fabric moulds that allow optimised forms to be cast. The  
40 permeability of fabric moulds (which are typically made using geotextiles) allows  
41 excess water and trapped air to escape, resulting in a more durable surface finish  
42 with a denser and more tightly packed microstructure (Orr et al., 2013). In addition,  
43 fabric formwork is reusable in most cases, with the fabric geometry able to form a  
44 different element by an adjustment of its specific tension and clamping (Chandler and  
45 Pedreschi, 2007).

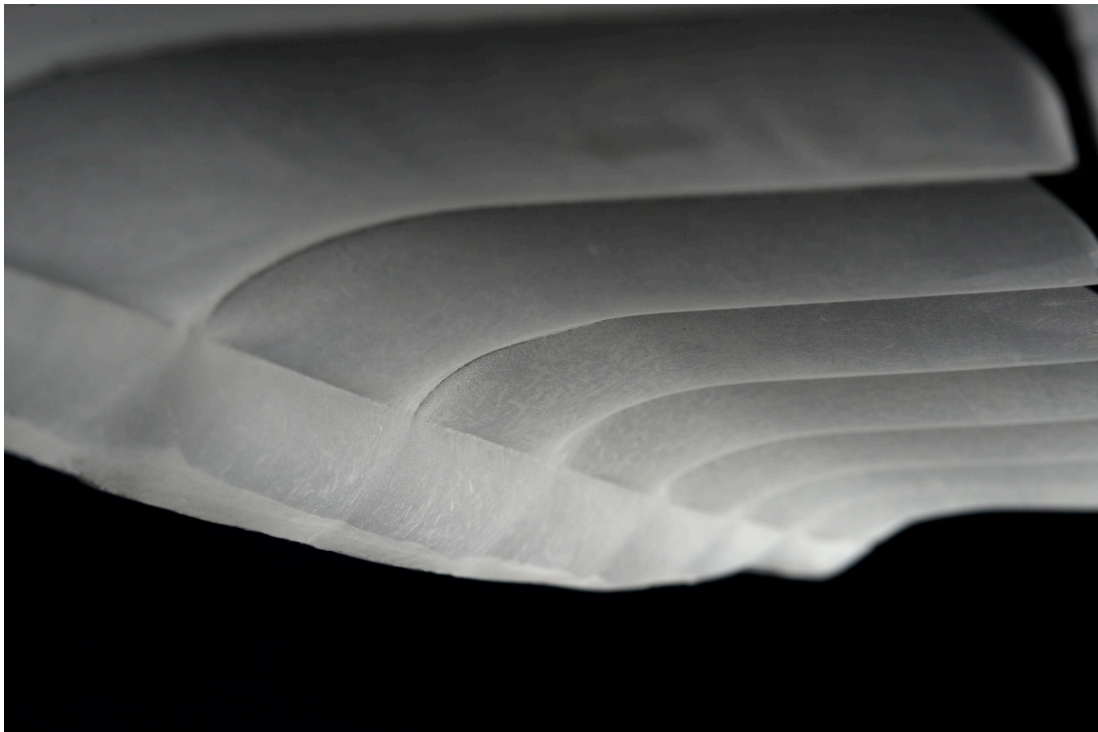
46 Permeability is widely believed to influence the propensity for heat-induced explosive  
47 concrete spalling (Klingsch, 2014). Since permeable formwork typically reduces the  
48 porosity of the cast face, the extent to which a fabric formed surface layer may alter  
49 the tendency for a concrete sample to spall is unknown. Indeed, like-for-like tests  
50 performed on the same concrete mix but with differing surface porosity can help to  
51 unpick the relative importance of pore-pressure effects versus differential thermal  
52 effects as drivers for heat-induced spalling of concrete.

53 Severe thermal exposure testing undertaken at the University of Edinburgh using the  
54 bespoke Heat-Transfer Rate Inducing System (H-TRIS) aimed to observe potential  
55 differences in propensity for heat induced spalling, whilst also observing internal  
56 temperatures and differential thermal displacements to evaluate the effects of casting  
57 with a permeable mould on high temperature performance of concrete. Further  
58 testing involved a study of the pore structure of fabric and timber-formed cast  
59 concrete surfaces using a scanning electron microscope (SEM).

## 60 2 Literature review

### 61 2.1 Flexible formwork

62 Fabrics have been an integral part of permeable mould formwork since the 19<sup>th</sup>  
63 century. It wasn't until the late 1980s, however, that research into synthetic fabrics  
64 resulted in high strength, tear resistant, and economical materials for this purpose.  
65 This led in turn to new methods of concrete construction for offshore, hydraulic, and  
66 coastal engineering environments (Veenendaal et al., 2011). More recent research  
67 into the use of permeable moulds has explored its use for structural optimisation,  
68 geometric form finding, and enhanced constructability (Hawkins et al., 2016). Figure  
69 1 shows an example of a structurally optimised beam designed to minimise material  
70 and self-weight whilst maximising flexural strength.



71  
72 **Figure 1: Fabric formed concrete beam optimised for flexural strength.**

73

### 74 2.1.1 Concrete properties

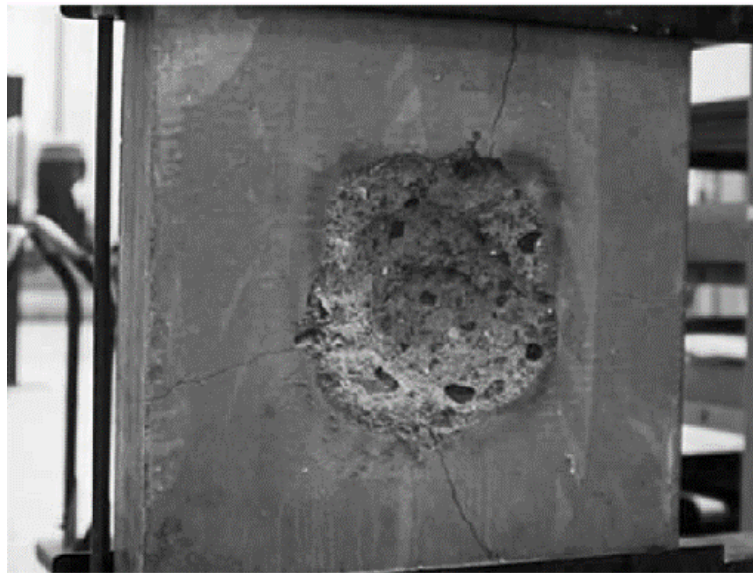
75 When cast into permeable formwork, excess water in the concrete in a zone of  
76 approximately 0-15mm from the cast surface can escape (Orr et al., 2013). The  
77 water to cement ratio in this zone is thereby reduced (by around 35%, depending on  
78 the fabric porosity (Orr et al., 2011, Frank, 2015)). This provides a localised increase  
79 in surface strength of as much as 80% (Frank, 2015), a higher density, and lower  
80 permeability (Orr et al., 2013). Furthermore, any air trapped in the formwork is also  
81 able to escape (Chandler and Pedreschi, 2007). Combined, these two mechanisms  
82 result in a significantly improved quality of the cast face.

83 The local increase in strength and reduction in permeability at the surface of the cast  
84 material also leads to improvements in durability. Orr et al. (2013) showed 50%  
85 average reductions in carbonation and chloride ingress, for fabric formed concrete,  
86 reinforcing similar research carried out by Price (2000) on controlled permeability  
87 formwork (CPF). If there are smaller pores and a reduced volume of interconnected  
88 pores present in the concrete surface layer, it is anticipated to increase the  
89 propensity for heat-induced explosive concrete spalling. A reduction in porosity will  
90 prevent the expulsion of gases (including pore moisture) through the surface layer at  
91 high temperatures, thereby potentially increasing the likelihood of spalling, further  
92 exacerbated by high strength concrete which is known to be more susceptible to  
93 spalling (Khoury, 2000).

## 94 2.2 Spalling

95 Khoury (2000) described spalling as the process of concrete breaking off from a  
96 structural member, during high temperature states, in a violent or non-violent nature.  
97 Although research has been conducted on spalling since at least the 1910s  
98 (Klingsch, 2014), spalling remains an incompletely understood phenomenon within

99 the scientific community – and is currently impossible to predict with confidence. An  
100 example of severe heat-induced concrete spalling is shown in Figure 2, where only  
101 the spalled area was exposed to heating during the test. A loss of structural material  
102 is evident, which reduces the volume of the element and could result in failure  
103 through loss of cross section or loss of thermal protection to the internal steel  
104 reinforcement.



105  
106 **Figure 2: Severe heat-induced explosive spalling of a concrete sample locally exposed to elevated**  
107 **temperature (Hertz, 2003b).**

108  
109 According to Jansson (2008), prominent researchers in the late 20<sup>th</sup> Century Meyer-  
110 Ottens (1972) and Copier (1979) hypothesised that the probability of spalling is low if  
111 the moisture content of concrete is also low. Mindeguia et al. (2011) proposed that  
112 free and physically bound water holds the core responsibility over the development of  
113 internal pore pressures from elevated temperatures. Considering moisture as an  
114 important factor affecting the propensity for concrete spalling, it is therefore clearly  
115 detrimental to have a large amount of free water within a sample.

116 The Moisture Clog Model originally developed by Harmathy (1965) describes one of  
117 two widely accepted theoretical mechanisms for spalling. At elevated temperatures, a  
118 plane of fully saturated concrete is expected to form within the concrete specimen, as  
119 a result of vaporisation of pore water within the concrete, restricting the movement of  
120 steam out of the sample. This causes pore pressures within the concrete to rise.  
121 Once the tensile strength of the concrete is exceeded locally, spalling may occur  
122 (Jansson, 2013). By cutting specimens shortly after they been tested at high  
123 temperature Jansson (2013) demonstrated that a moisture clog layer was visible,  
124 which partly validated this explanation of pore pressure as a factor influencing  
125 spalling. Although the mechanism has not been definitively proven and the research  
126 community has put forward various alternative mechanisms (Khoury, 2000), the  
127 Moisture Clog theory is still regarded as relevant to explaining the phenomenon of  
128 spalling. The other key mechanism involves differential thermal stresses which are  
129 generated as the concrete surface heats and tries to expand, whereas the cooler  
130 concrete within the core remains cool; this generates differential thermal stresses  
131 which are also thought to influence spalling. Indeed many researchers now feel that  
132 Thermal Stress Spalling is more important than Pore Pressure Spalling in many  
133 applications (Zhang and Davie, 2013).

134 In addition to moisture content, there are many further factors expected to influence  
135 spalling. These varied and complex factors range from the mix properties of the cast  
136 concrete to the geometry of the specimen, external loading, restraint conditions, and  
137 the heating rate (Jansson, 2008).

138 A brief explanation of spalling related factors directly linked to the testing undertaken  
139 in the current paper are given in Table 1; the risk related to spalling is after Klingsch  
140 (2014).

141

142

**Table 1: Spalling factors and their associated risk (after Klingsch, 2014)**

<b>Factor</b>	<b>Risk of spalling</b>	<b>Influence</b>
<b>Silica fume content</b>	Very high	Testing by Hertz (2003) showed that the mixes between the cement grains leads to a higher propensity for explosive spalling.
<b>Permeability</b>	High	Directly affects the release of vapour pressures, and so with low permeability, gasses have difficulty escaping and the risk of spalling is increased.
<b>Type of aggregate</b>	Variable	Limestone is based on carbonates and has a higher heat capacity with low thermal expansion, compared to siliceous aggregates (Kodur and Phan, 2007).
<b>Aggregate size</b>	Moderate	Connolly (1995), cited by Klingsch (2014), states that larger aggregates moderately increase the risk of spalling due to such mixes having inferior surface/mass ratios.
<b>Compressive strength</b>	High	Permeability reduces with increased strength/density from a lower water/cement ratio, thus increasing the risk of explosive spalling (Kodur and Phan (2007).

143

144

145

146

147

148

149

150

151

152

153

Extensive research has been performed with the aim of minimising, and ultimately preventing, heat-induced explosive concrete spalling (Zeiml et al., 2006). A common method of spalling mitigation is by adding polypropylene (PP) anti-spalling fibres to a concrete mix. Research suggests that at around 170°C the PP fibres melt, creating channels through the concrete matrix and altering the microstructure by increasing its porosity (Klingsch, 2014). Water vapour formed during high temperature can therefore be more easily expelled, and the build-up of internal pore pressures is reduced (Lura and Terrasi, 2014). It is noteworthy that this theory of PP anti-spalling fibres' mechanism of functioning has yet to be fully validated, and it remains a topic of some controversy.

154

### **2.3 Structural fire testing**

155

156

157

Full-scale fire tests of real buildings are rare, with a few notable exceptions such as Cardington (Kirby, 1997). In general engineers must rely on smaller-scale standard furnace testing to develop design guidance for spalling. In 1918, the first

158 standardised test method was published: ASTM C19, now redesignated as ASTM  
159 E119 (2016) (Grosshandler, 2002) which included the innovation of a prescribed  
160 time-temperature curve (Lawson et al., 2009). Despite fundamental pitfalls in the  
161 ability of ASTM E119 (2016) to demonstrate/validate the fire resistance of real  
162 structures in real fires, its fundamental testing formula remains essentially unchanged  
163 since 1918 (Maluk and Bisby, 2012). The current British Standard BS EN 1992-1-2  
164 (2004) for fire safety structural design of concrete structures has been developed  
165 from the same principles of ASTM E119 (2016) and so also contains time-  
166 temperature curves.

### 167 *2.3.1 Furnace testing limitations*

168 Standard fire resistance testing in furnaces has some significant limitations.  
169 Researchers sometimes test multiple specimens simultaneously, leading to over-  
170 instrumentation while the exposed thermal environment is partly ignored (Maluk et  
171 al., 2012). Due to the comparatively high cost for furnace testing, a limited number of  
172 tests can typically be performed, which results in an inability to perform repeat testing  
173 or any statistical analysis, and making a reliability-based approach to design  
174 impossible (Maluk et al., 2012). In addition, furnace testing has comparatively poor  
175 repeatability, and the thermal energy that the specimen absorbs over time is only  
176 indirectly controlled by making measurements of gas temperatures within the  
177 furnace, as opposed to heat absorbed into the test samples (Maluk and Bisby, 2012).  
178 It can thus be difficult to accurately quantify the thermal loading a specimen receives  
179 within a furnace (Maluk et al., 2012).

### 180 *2.3.2 Heat-Transfer Rate Inducing System (H-TRIS)*

181 A novel thermal testing method has been developed at the University of Edinburgh  
182 (Maluk et al., 2016) called The Heat Transfer Rate Inducing System (H-TRIS) (Figure

183 3). This consists of four high performance propane-fired radiant heaters (to provide  
184 thermal loading), mounted on a mechanical linear motion system. When testing using  
185 H-TRIS the thermal exposure is controlled directly by controlling the heat flux the  
186 specimen is exposed to during testing as opposed to the controlling the temperature  
187 within the furnace in standard tests (Hulin et al., 2015). A heat flux gauge is used to  
188 measure and calibrate the incident heat flux from the radiant panels at the surface of  
189 the tested element, and the position of the radiant panels from the sample face is  
190 varied so as to simulate the desired time-history of thermal gradients within the  
191 sample. If desirable to compare results to those of standard furnace tests, the  
192 thermal exposure equivalent to the thermal exposure that samples experienced  
193 during a specific standard furnace test can be calculated. This is done using through  
194 thickness temperatures from samples tested in the furnace and an inverse heat  
195 transfer model; the result being the equivalent incident heat flux versus time curve.  
196 Before testing, the incident heat flux is measured using a Schmidt-Boelter heat flux  
197 gauge at different offset distances from the radiant panels. Thermal exposure is then  
198 controlled by controlling the distance between the radiant panels and sample in  
199 accordance with this calibration

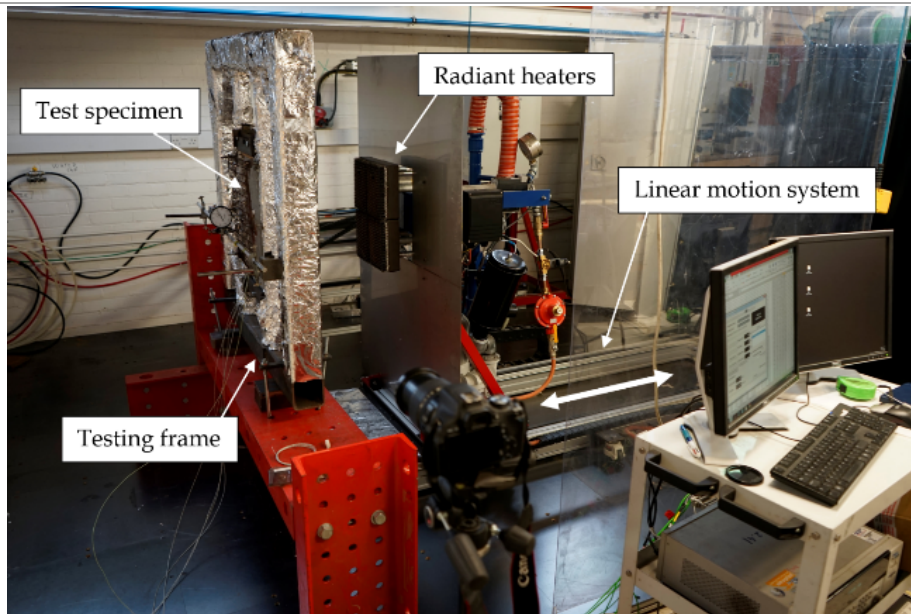


Figure 3: An overview of the H-TRIS testing apparatus at The University of Edinburgh.

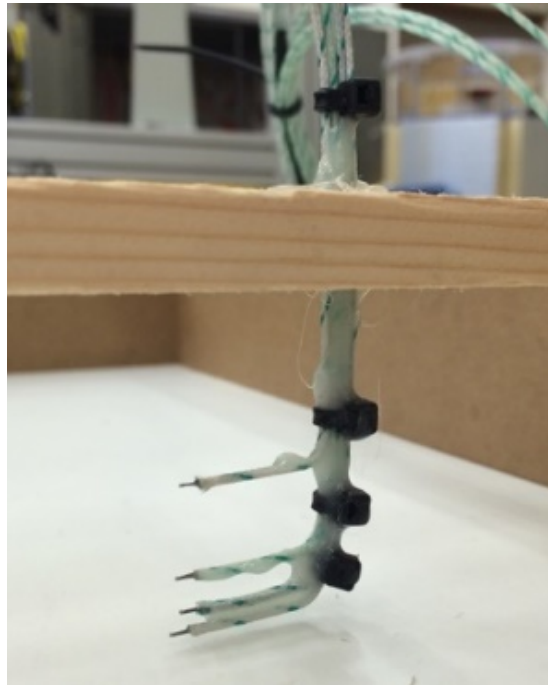
### 3 Test methodology

To investigate and compare the spalling behaviour of concrete cast in permeable versus impermeable moulds, a total of six prismatic concrete test samples, with dimensions 500mm x 200mm x 45mm, were cast for testing using the H-TRIS methodology and apparatus.

#### 3.1 Sample construction

Three samples were cast with permeable formwork on one face, and three were cast within impermeable moulds. Two additional samples (one of each mould type) were cast for later analysis using scanning electron microscopy (SEM). Nine 100mm cubes were also cast alongside the samples for mix characterisation purposes. All test samples were internally instrumented with five 0.3mm diameter welded tip insulated fibreglass (Type K) thermocouples (see Figure 4), with their tips carefully placed (+/- 2mm) at depths of 2mm, 5mm, 10mm, 22mm and 45mm from the face exposed to heating. These were placed using a thermocouple tree arrangement (as shown in Figure 4) which was cast inside the samples during casting operations. The

217 fifth thermocouple was placed on the back face of each specimen during testing,  
218 covered by ceramic insulation and sealed in place using aluminium tape.



219

220 **Figure 4: Thermocouple tree restrained in place within the formwork prior to casting the samples.**

221

222 The mix design used in the current study (see Table 2) had a 28-day design  
223 compressive cube strength of 60MPa. This compressive strength was chosen as it is  
224 a realistic strength that is used in permeable concrete formwork building construction.

225 All concrete was mixed in the Concrete Laboratory at the University of Bath, following

226 The Silica Fume Association (2011) guidance for casting with silica fume. All samples

227 and cubes were cured in accordance with BS EN 13670 (2009b). All samples were

228 weighed 48 hours after casting. The samples were transported to Edinburgh and

229 tested 90 days after casting. The fabric used was HaTe PES 70/70, with a

230 characteristic opening size of  $0.1 \times 10^{-3}$  m.

231

232

233

234

Table 2: Concrete mix design

Material	Amount
Cement CEM I 42.5 R (kg/m <sup>3</sup> )	400
Coarse aggregates (4-20mm) (kg/m <sup>3</sup> )	1000
Fine aggregates (0-4mm) (kg/m <sup>3</sup> )	840
Superplasticiser (l/m <sup>3</sup> )	4
Water (l/m <sup>3</sup> )	180
Silica fume (kg/m <sup>3</sup> )	40
Unit weight, $\gamma_{c, \text{mix A}}$ (kg/m <sup>3</sup> )	2464
28 day compressive strength, $f_{c,28}$ (MPa)	60
Water/cement ratio	0.41

235

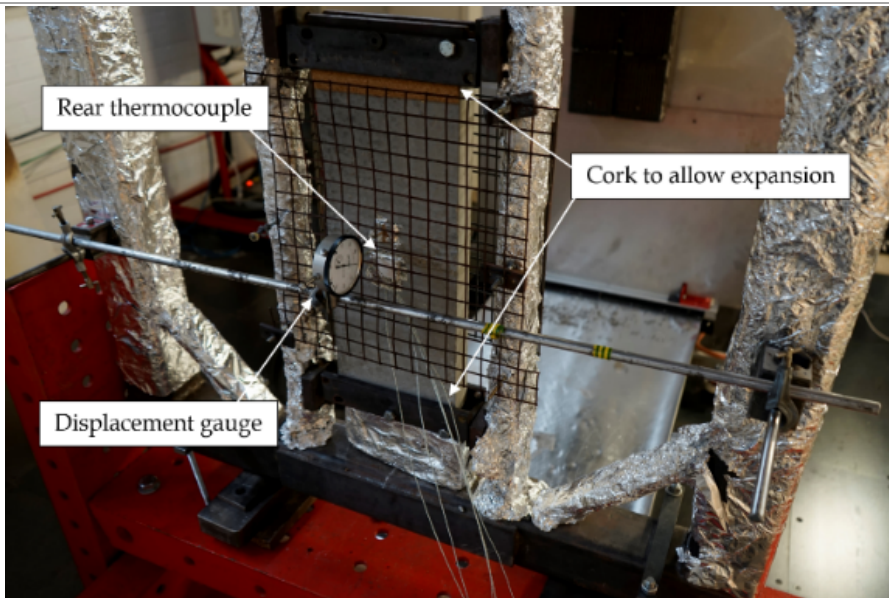
### 236 3.2 Test setup

237 The test set up for the spalling tests is shown in Figure 5 and Figure 6. Specimens  
 238 were placed into a supporting test frame, with cork placed underneath each concrete  
 239 sample to prevent them from moving during heating. However, the concrete  
 240 specimens were not mechanically restrained, thus allowing free thermal expansion  
 241 and bowing during testing.

242 Research has shown that the application of an appropriate external load or restraint  
 243 can influence spalling (Hertz and Sørensen, 2004, Rickard et al., 2017). However,  
 244 since this is a pilot study, the parameters being investigated were kept to a minimum  
 245 and a loading frame was not used for these samples.

246 A displacement gauge was attached at the centre of the back face of the specimens.  
 247 The back face of the sample was covered by a wire mesh to protect the  
 248 instrumentation in case of rear-face spalling (which had been observed in similar  
 249 prior testing at Edinburgh (Hulin et al., 2015). Two magnetic clamps held the cross  
 250 bar for the displacement gauge, as shown in Figure 5, and a camera was used to  
 251 record the displacement gauge reading for later transcription.

252 Figure 6 shows H-TRIS in its warmup and test preparation phase. To protect each  
253 sample during warmup of the radiant panels until they reached a steady-state heat  
254 flux condition, insulation was placed in front of the specimens. Upon reaching a  
255 homogenous heat flux, the tests were initiated by removing the protective insulation  
256 board. Each test was programmed to follow a specific time versus incident heat flux  
257 curve (as shown in Figure 7). Two different heating curves were used: (1) an ISO 834  
258 (2002) equivalent fire curve; and (2) a modified hydrocarbon (HCM) (BS EN 1991-1-  
259 2, 2002) equivalent heating curve. To follow these curves a calibration curve was  
260 used to guide the location of the H-TRIS radiant panels as they moved towards the  
261 test specimen. For calibration curve 1, the heat flux gauge was placed in line with the  
262 centre of the four-panel heating assembly. For calibration curve 2, the heat flux  
263 gauge was placed in line with the centre of one of the four radiant panels from which  
264 the overall radiant panel array was fabricated. Following the completion of each test,  
265 each sample was weighed, allowing the calculation of moisture lost during testing  
266 (note that no mass was lost due to spalling, since no spalling was observed for any of  
267 the samples).

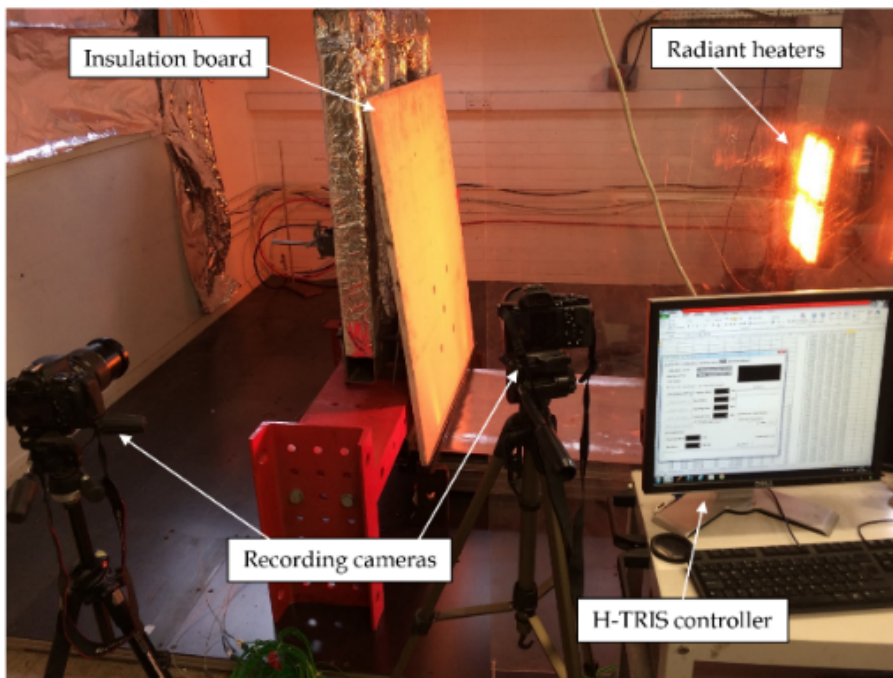


268

269

270

Figure 5: *Restraint conditions and displacement gauge arrangement for concrete sample testing in H-TRIS.*

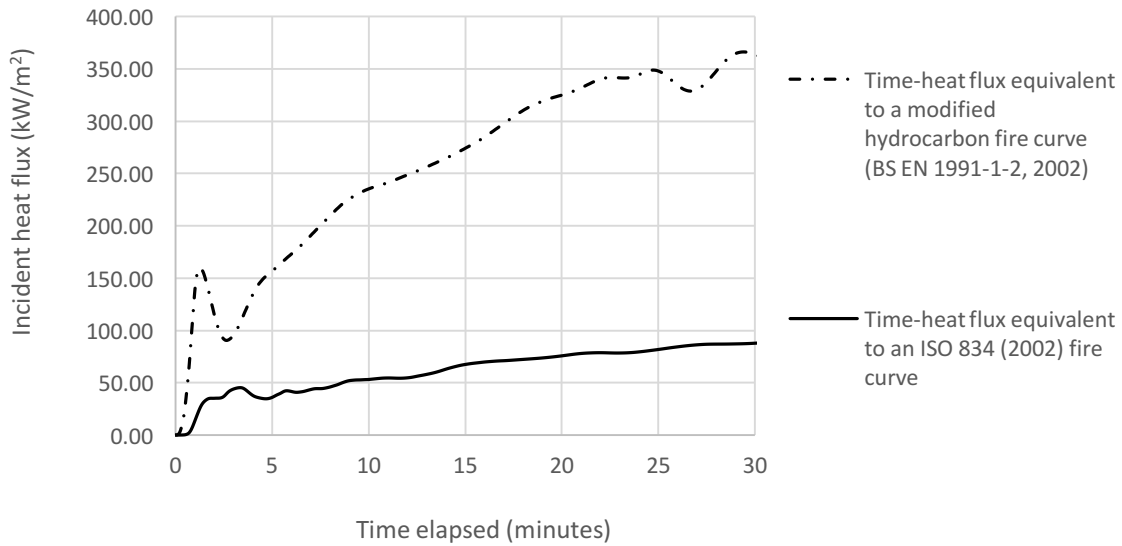


271

272

273

Figure 6: *H-TRIS preparation phase, showing radiant panel array (left) and protective insulation board (centre).*



274

275

**Figure 7: Time versus incident heat flux equivalent curves used for testing to both ISO and HCM heating curves.**

276

277

**4 Test results**

278

**4.1 Concrete properties**

279

The average concrete compressive strength, measured from three cubes and tested in accordance with BS EN 12390-3 (2009a), was 68MPa on the test date (90 days after casting).

280

281

282

**Table 3: Mass and calculated elastic modulus of each concrete test sample.**

Sample name	Mass 48 hours after casting (kg)	Calculated unit mass (kg/m <sup>3</sup> )
AT2	10.857	2412.67
AT3	11.238	2497.33
AT4	11.489	2553.11
AF2	11.099	2466.44
AF3	10.976	2439.11
AF4	11.017	2448.22

283

284 **4.2 H-TRIS testing results**

285 Table 4 summarises the results from all H-TRIS tests; as already noted, no spalling  
286 was observed for any of the samples.

287

288  
289

Table 4: Summary of H-TRIS results

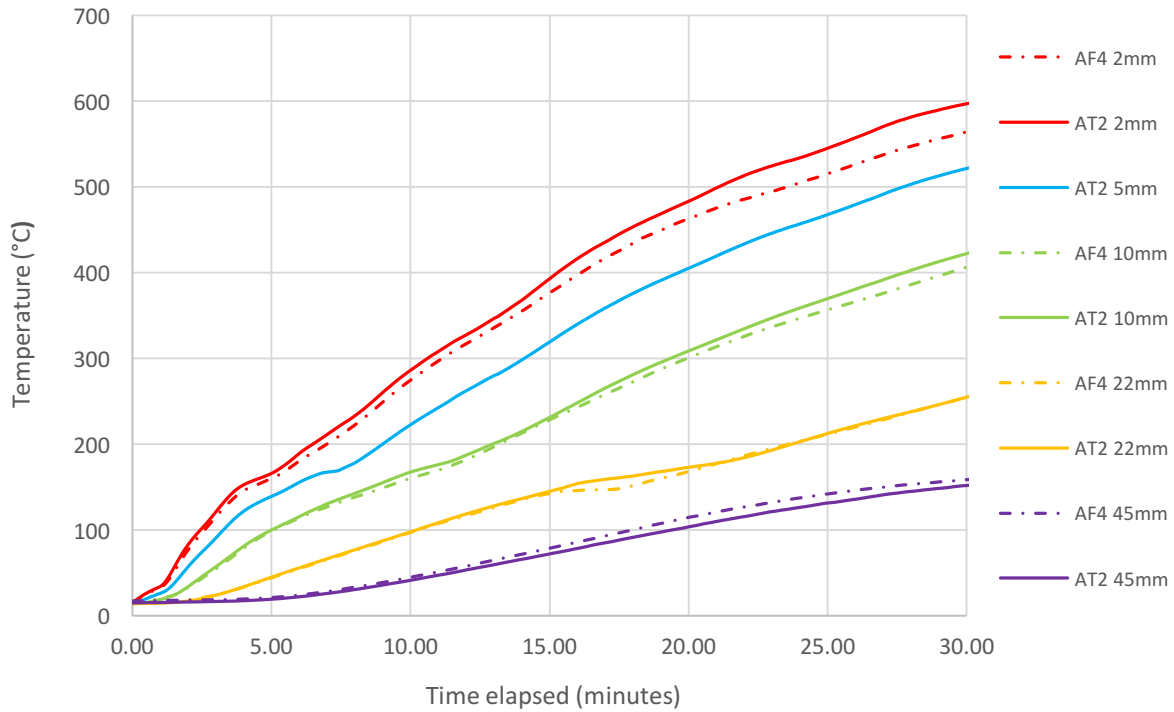
Sample	Concrete mix	Timber /fabric face	Equivalent heating curve (see Figure )	Calibration curve (see Error! Reference source not found.)	Minimum sample distance (mm)	Max heat flux (kW/m <sup>2</sup> )	Spalling observed	Heating time recorded (minutes)	Cooling time recorded (minutes)	Comments	
AT2	A	Timber	ISO 834 standard fire		1	195	88	None	30	0	All thermocouples working correctly. Peak displacement estimated, no full displacement/ time data.
(AT3)	A	Timber	Modified hydrocarbon fire		1	48	197	None	7	N/A	Test failed after 7 minutes due to maximum heat flux required by heating curve exceeding maximum calibrated heat flux from the selected calibration curve. Displacement gauge failure. Data incomplete.
AT3 Retest	A	Timber	Modified hydrocarbon fire (max 162 kW/m <sup>2</sup> )		1	97	162	None	30	0	All thermocouples working correctly. Specimen starting temperature around 70°C due to re-test. Displacement data incomplete.
AT4	A	Timber	Modified hydrocarbon fire		2	96	180	None	25	35	H-TRIS malfunction after around 25 minutes of heating. Further heating aborted. All thermocouples working correctly.
AF2	A	Fabric	Modified hydrocarbon fire (max 162 kW/m <sup>2</sup> )		2	102	162	None	30	30	All thermocouples working correctly. Full data set collected.
AF3	A	Fabric	Modified hydrocarbon fire		2	96	180	None	25	30	H-TRIS malfunction after around 25 minutes of heating. Further heating aborted. All thermocouples working correctly.
AF4	A	Fabric	ISO 834 standard fire		1	195	88	None	30	0	5mm thermocouple not functioning.

290  
291

N.B. 5mm temperature recordings for sample AF3 featured occasional sporadic jumps and so data has been selectively removed from Figure 9 and Figure 10.

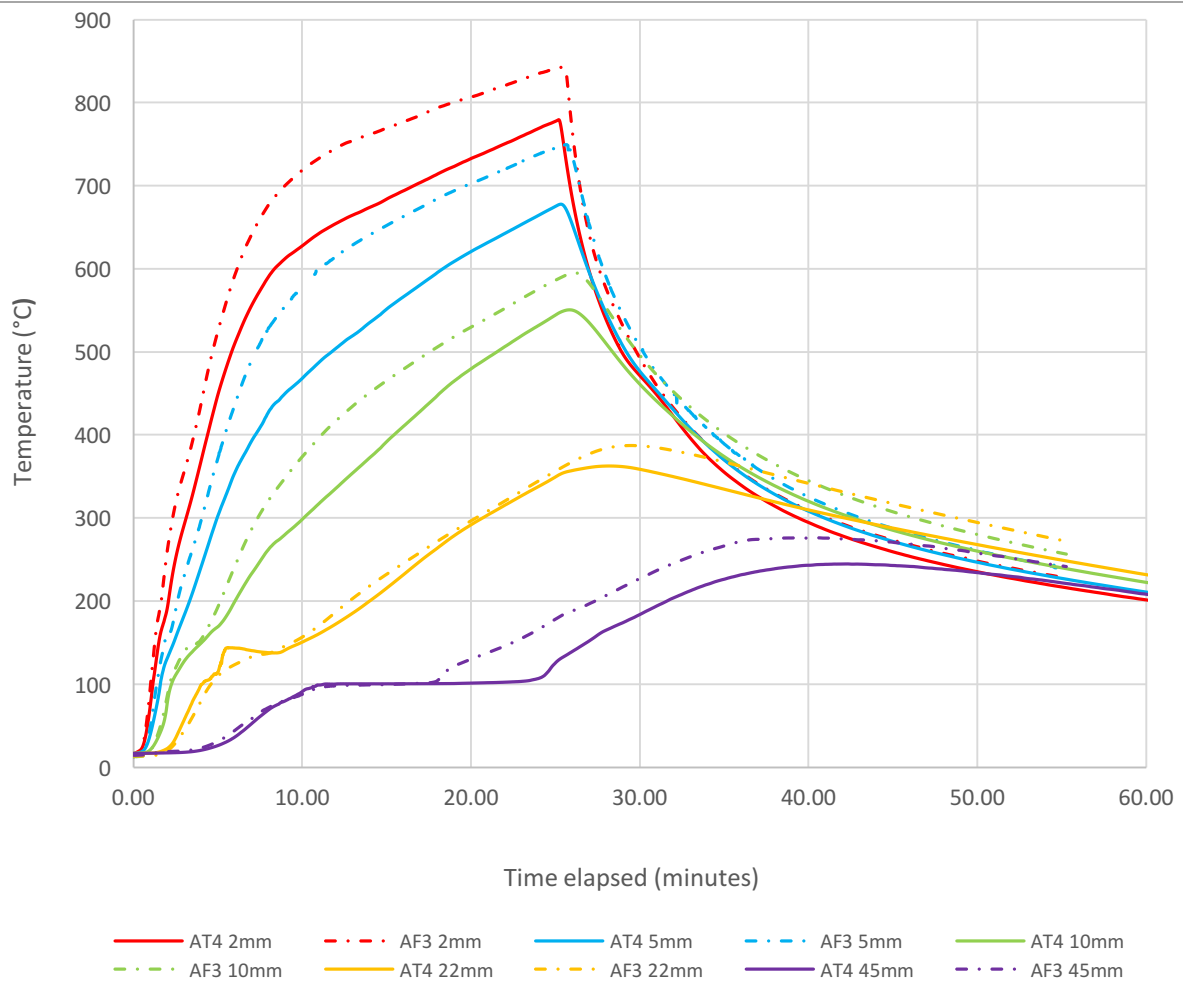
292 4.2.1 Temperature readings

293 The recorded temperatures from selected H-TRIS tests are shown in Figure 8 to Figure  
294 10.



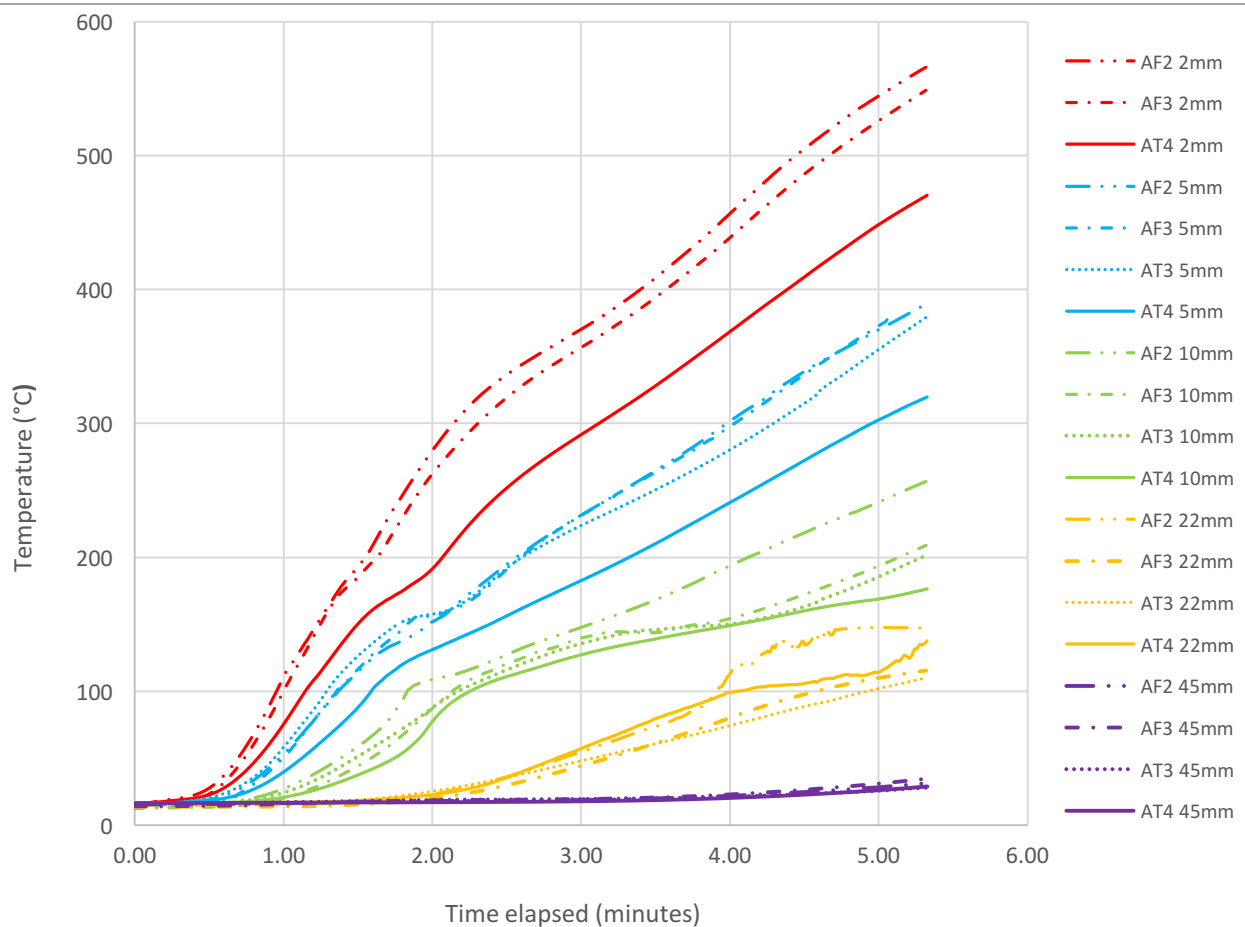
295 **Figure 8: Temperatures recorded in H-TRIS tests on AT2 and AF4 (simulated ISO 834 heating)**

296  
297  
298 Figure 8 shows similar and comparable temperature curves from both the traditionally cast  
299 sample, AT2, and the sample formed using a permeable mould, AF4. The front  
300 thermocouples, cast at 2mm (+/- 2mm) display a small difference in temperature most  
301 likely due to human error from placement. At the middle of both sections, 22mm (+/-2mm),  
302 temperature readings are consistent with one-another. The rear face thermocouples  
303 display alike readings.



304  
305 **Figure 9: Temperatures recorded in H-TRIS tests AT4 and AF3 (simulated HCM heating up to 162 kW/m<sup>2</sup>)**

306  
307 Figure 9 shows that at all thermocouple depths, temperatures are greater within the  
308 sample formed from a permeable mould, AF3, than the sample formed from traditional  
309 timber shuttering, AT4. This data suggests that the whole thermocouple tree from sample  
310 AF3 is positioned closer to the thermally loaded surface than AT4, or the thermocouple  
311 tree from AT4 is positioned further away from the thermally loaded surface than AF3.



312  
 313 **Figure 10 Temperatures recorded during H-TRIS testing on AT3, AT4, AF2 and AF3 (simulated HCM fire up to**  
 314 **162 kW/m<sup>2</sup>)**

315  
 316 Figure 10 incorporates temperature data from two samples formed from permeable  
 317 moulds and from two traditionally cast samples. Similarly to Figure 9, permeably formed  
 318 samples reach greater temperatures when studying the output from the 2mm, 5mm and  
 319 10mm (+/- 2mm) thermocouples. This trend does not continue with temperature readings  
 320 from the 22mm and 45mm (+/-2mm) thermocouples, suggesting human error with  
 321 placement of thermocouple trees.

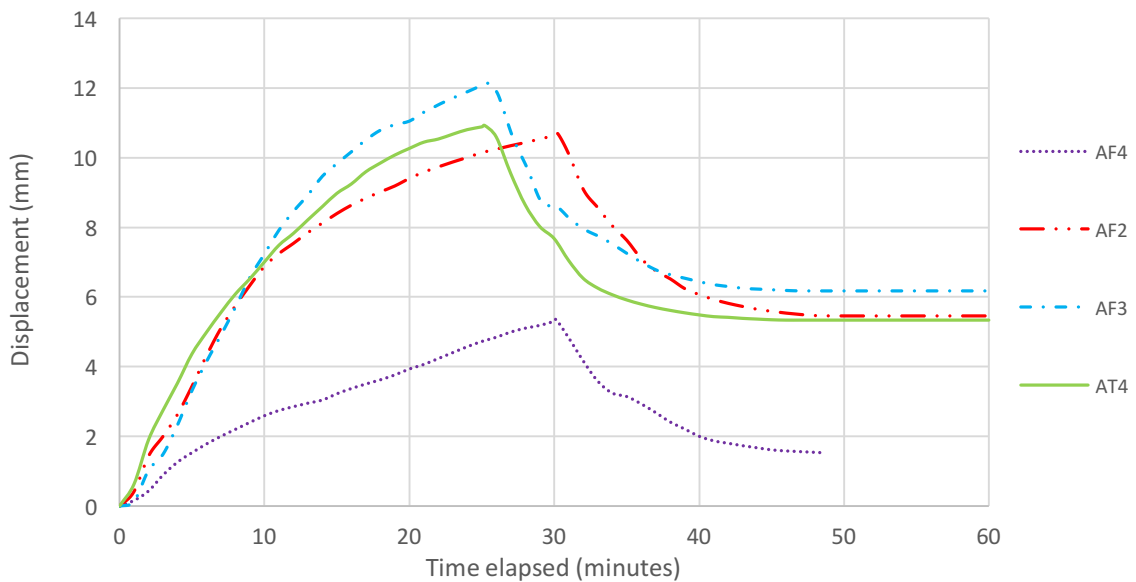
322 **4.2.2 Sample displacements**

323 All tests were performed with samples unloaded and unrestrained against curvature and  
 324 end rotations. This resulted in high differential thermal stresses causing deflection (thermal  
 325 bowing) of all concrete samples during heating. All concrete samples bowed outwards, i.e.

326 in the direction of the heat source (Figure 11). Data is presented in Figure 12). Samples  
327 AF3 and AT4 both experienced the same H-TRIS testing regime (modified hydrocarbon  
328 fire) while sample AF4 experienced a ISO 834 fire and AF2 experienced a modified  
329 hydrocarbon fire limited to 162 kW/m<sup>2</sup>. Differences in displacement are likely due to  
330 measurement error from thermal sources.



331  
332 **Figure 11: Post-test thermal bowing of Concrete Sample AT3.**



333  
334 **Figure 12: concrete sample mid-height lateral displacements during heating**

335 **4.3 Mass-loss from dehydration**

336 Table 5 shows the mass loss from the dehydration of each sample due to fire testing. The  
 337 range of specimen moisture contents lie between 5.41% and 8.41%. AT2 and AF4 have  
 338 the lowest moisture content of all six samples after testing. Since these samples were  
 339 exposed to the less intense ISO 834 (2002) equivalent curve, it is possible that thirty  
 340 minutes of heating did not fully dry out both samples and so a value of moisture loss by  
 341 mass has also been presented.

342 Thermal testing of 66 comparably sized specimens undertaken using H-TRIS by Maluk et  
 343 al. (2013) resulted in all specimens apart from one mix set experiencing spalling. All those  
 344 specimens at the time of testing had moisture contents between 4.0% to 5.0% (by mass).  
 345 This comparison indicates that the moisture content of the samples tested in this paper are  
 346 not dominant factors for the absence of spalling. The specimens tested by Maluk et al.  
 347 (2013) had higher compressive strengths (103-112 MPa) and experienced greater restraint  
 348 conditions with compressive stress applied to half of the specimens. A further discussion  
 349 of factors influencing spalling such as these is presented in Section 5.

350 **Table 5: Measured mass-loss from dehydration of the concrete samples during testing.**

Sampl e	Casting date	Mass 48 hours after casting (kg)	Post-test mass (kg)	Moisture loss by mass (%)	Moisture content (%)
AT2	09/12/2015	10.857	10.218	5.89	6.25
AT3	09/12/2015	11.238	10.366	7.76	8.41
AT4	09/12/2015	11.489	10.711	6.77	7.26
AF2	09/12/2015	11.099	10.332	6.91	7.42
AF3	09/12/2015	10.976	10.129	7.72	8.36
AF4	09/12/2015	11.017	10.452	5.13	5.41

351

## 352 **5 Analysis**

353 None of the samples tested showed any heat-induced explosive concrete spalling.  
354 Possible reasons for this are discussed below.

### 355 **5.1 Concrete strength**

356 Kodur and Phan (2007) stated that strengths over 70 MPa have a higher propensity to  
357 spall. Maluk et al. (2013) tested concrete samples of an identical size to those in this paper  
358 (500mm x 200mm x 45mm) using H-TRIS. High performance self-consolidating concrete  
359 (HPSCC) was used with a design strength class of C90. Out of 11 mixtures each with  
360 varying PP fibre types and quantity, four mixes spalled. This demonstrates that even with a  
361 considerably higher strength, spalling tends to display an element of randomness and is  
362 influenced by other factors in addition to the strength class, even with carefully controlled  
363 testing and thermal exposures, thus underlining a lack of understanding of the risk of  
364 spalling and the mechanisms contributing to spalling.

### 365 **5.2 Restraint conditions**

366 During testing, all samples were unrestrained at their ends. They all exhibited large bowing  
367 under heating due to the high through-thickness thermal gradient created by heating from  
368 one side of the specimen. Their lack of restraint, and ability to deform, may have  
369 contributed to the absence of spalling. Hertz (2003) demonstrated that for samples  
370 restrained in place with fixed ends, it is more difficult for specimens to relieve internal  
371 thermal stresses through deflection, making restrained specimens more likely to spall.

### 372 **5.3 Applied loading**

373 All specimens in this paper were tested without externally applied static loads. The  
374 addition of a moderate amount of compression has been shown to increase the likelihood  
375 of spalling. Carré et al. (2013) exposed specimens with a concrete strength of 37MPa to

376 an ISO 834 (2002) time-temperature curve. With up to a 10MPa compression on these  
377 specimens, no spalling was recorded. At 15MPa compression, spalling was observed.

#### 378 **5.4 Thermal cracking**

379 A further underlying reason for the absence of spalling seen in this paper can be related to  
380 the extensive thermal cracking which developed during testing. As thermal cracks develop  
381 in normal density concrete without external load or restraint as was used here, stresses at  
382 the surface are relieved and the propensity for spalling is reduced (Hertz, 2003).

#### 383 **5.5 Summary**

384 The concrete samples cast using permeable moulds do not appear to be more susceptible  
385 to spalling under the conditions studied. There are no obvious differences in the  
386 temperature profiles or thermal curvatures from H-TRIS testing indicating that the  
387 increased surface durability gained from using fabric formwork does not increase the  
388 likelihood of spalling over traditionally formed concrete given the testing conditions. Slight  
389 variances in temperature readings can be accounted for by minor differences in the cast  
390 positions of thermocouples. As no spalling was observed, an investigation into the altered  
391 pore structure from permeable mould formed samples was undertaken using scanning  
392 electron microscopy.

393

#### 394 **6 Scanning electron microscopy**

395 To assess the porosity of concrete cast against timber and a permeable fabric, eight  
396 concrete samples of 25mm x 25mm x 25mm were cut from the centres of untested  
397 samples (four from an impermeably and four from a permeably cast sample). The cubes  
398 were set in epoxy resin under vacuum and polished to a high degree before imaging. No  
399 splutter coatings were applied to the sample. An example of a fabric formed surface  
400 sample is shown in Figure 13.

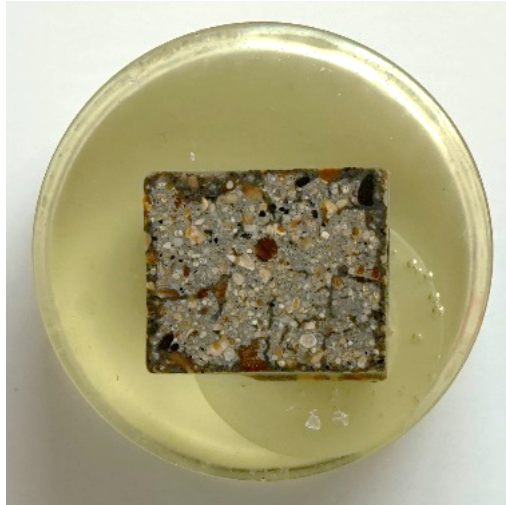


Figure 13: A polished fabric surface sample.

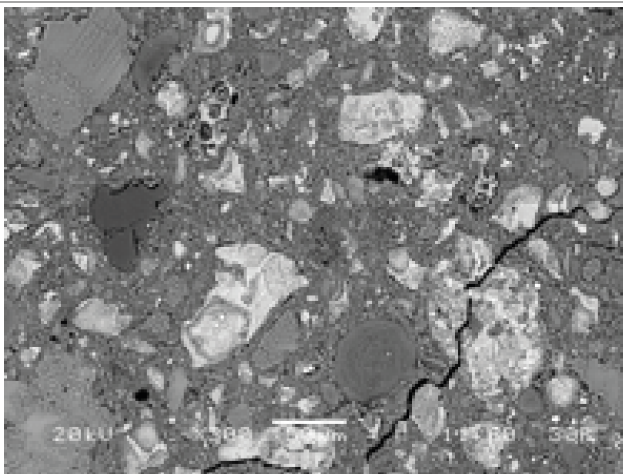
401

402

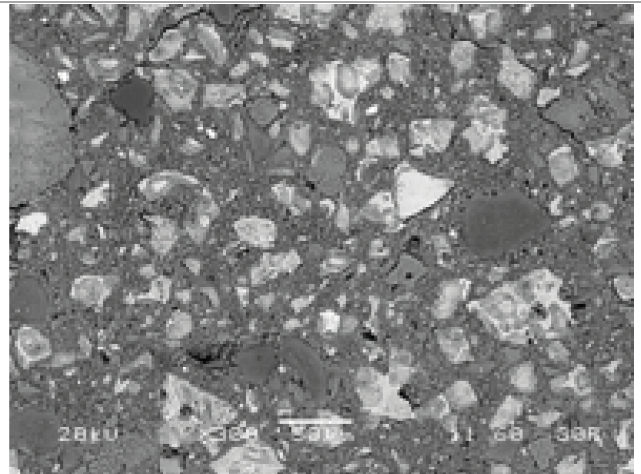
403 A JEOL SEM was used at the University of Bath for imaging. A range of backscattered  
404 electron images (BEI) were captured under low vacuum mode at 300x and 500x  
405 magnification. The samples were positioned with cast surface layer (permeable  
406 mould/timber) facing up at the microscope.

#### 407 **6.1 Scanning electron microscopy results**

408 BEI imaging taken from four concrete samples (permeable mould or timber: 'a' and 'b'  
409 samples taken from the same sample in different locations) are shown in Figure 14 -  
410 Figure 17. Voids are shown as black since the epoxy resin that filled the sample is very  
411 light in comparison to the concrete. Heavier minerals appear lighter. Frame positions for  
412 imaging were chosen with the aim of gathering a range of images from the cast surface  
413 layer.



(a)

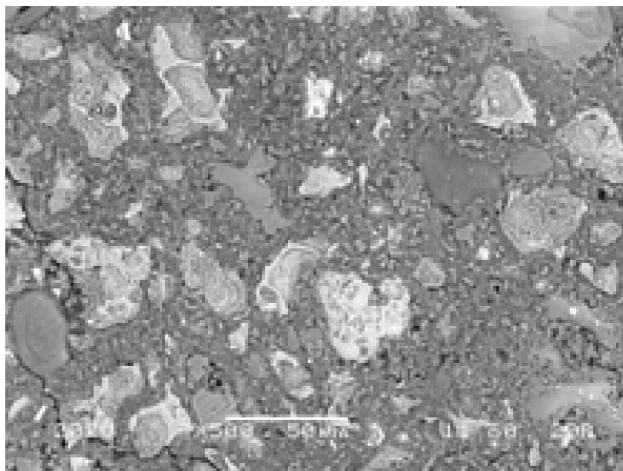


(b)

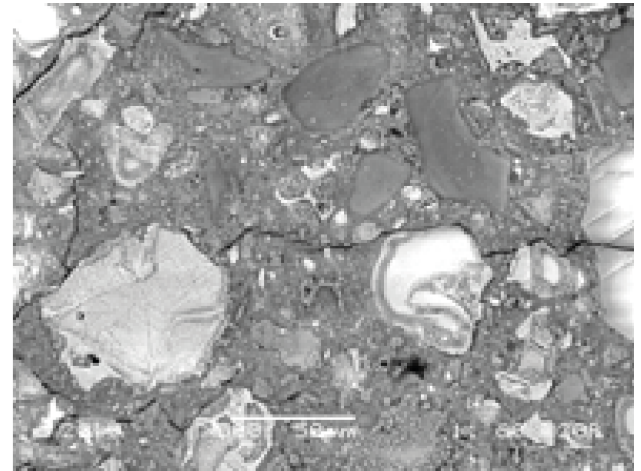
414

415

Figure 14: BEI (a, b) permeable mould surface at 300x magnification



(a)

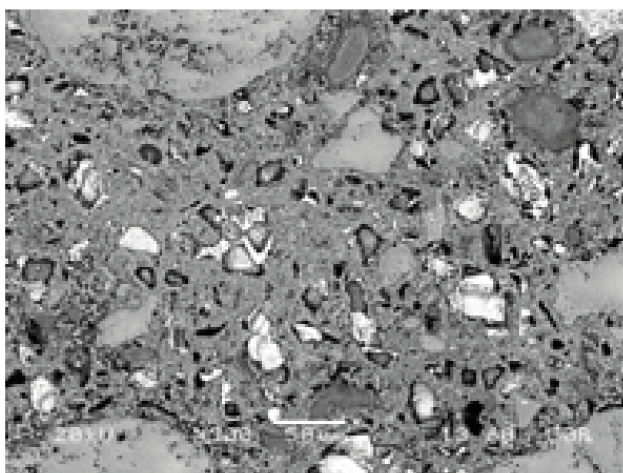


(b)

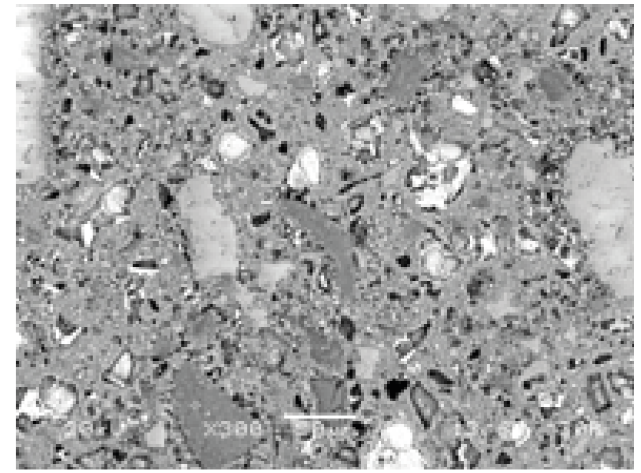
416

417

Figure 15: BEI (a, b) permeable mould surface at 500x magnification



(a)

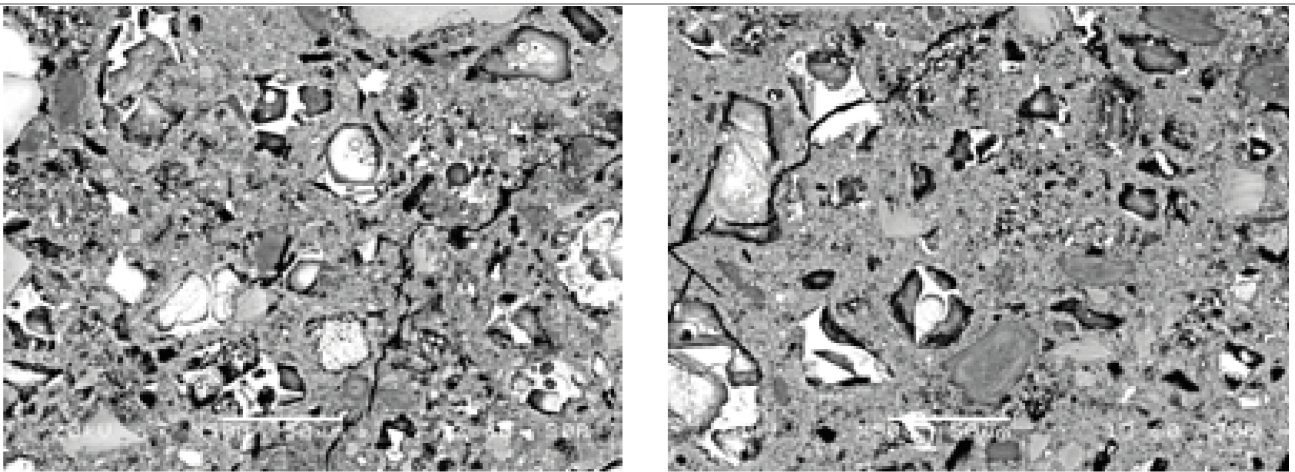


(b)

418

419

Figure 16: BEI (a, b) timber formed surface at 300x magnification



(a)

(b)

Figure 17: BEI (a, b) timber formed surface at 500x magnification

### 6.1.1 Image analysis

'ImageJ' analysis software (Ferreira and Rasband, 2011) was used to analyse the SEM imaging. To account for greyscale inaccuracies reproduced by the SEM, thresholding was performed using the 'analyse particles' function. For continuity one pore was selected per sample as a benchmark. To obtain a quantitative comparison of porosity, a particle analysis function was used to calculate the area of voids as a frame percentage. Original images were used with no cropping or removal of aggregates.

Table 6: Average voids ratio per surface finish at 300x and 500x magnification.

Surface finish	Magnification	Average void area (per frame as a %)
Fabric	300x	0.92
Timber	300x	3.81
Fabric	500x	0.47
Timber	500x	3.00

### 432 6.1.2 Summary

433 A stark difference is evident in the magnitude and distribution of pores between concrete  
434 formed from a permeable mould (Figure 14 and Figure 15) and a timber formed surface  
435 (Figure 16 and Figure 17). Table 6 shows the average voids area is over four times greater  
436 for a timber formed surface at 300x magnification, providing significant evidence of  
437 reduced porosity, and therefore, decreased permeability of a surface formed from a  
438 permeable mould. Orr et al. (2013) also demonstrated that a fabric formed surface layer  
439 contained a greater concentration of cement particles resulting in smaller and fewer  
440 interconnected pores. The higher density microstructure of the permeable mould concrete  
441 is further demonstrated by the large and frequent C-S-H gel formation, visible at 500x  
442 magnification, appearing as dark grey, by comparing Figure 15 and Figure 17).

## 443 7 Evaluation of experimentation

### 444 7.1 H-TRIS testing

445 Since all samples were tested unrestrained and unloaded, thermal expansion and bowing  
446 was expected. The boundary conditions tested simulate, for example, a concrete façade.  
447 To simulate a realistic structural load bearing scenario, the sample should be tested with  
448 axial and/or flexural restraint, and with representative loading applied.

### 449 7.2 Scanning electron microscopy

450 As a result of sample preparation, from polishing the surface of both the permeable mould  
451 and timber formed samples, the texture of the true outer layer was partially lost, and  
452 therefore, the backscattered electron images do not represent the exact surface layer.  
453 Section 6.1 still shows a distinct difference in the imaged surface layers and so, in the  
454 Author's opinion, the validity of the conducted microscopy remains.

## 455 **8 Conclusions**

456 The additional density and restricted permeability found by Orr et al. (2013) at the surface  
457 layer of fabric formed concrete revealed a potential hazard for the fire related performance  
458 of fabric formed concrete, specifically with relation to heat-induced explosive concrete  
459 spalling.

460 A pilot study, presented in this paper, was undertaken to examine this potential hazard.  
461 Fire testing undertaken at the University of Edinburgh using H-TRIS was inconclusive, with  
462 no observed spalling for concrete samples cast using conventional formwork or using  
463 permeable fabric formwork. Further research is required to draw definitive conclusions,  
464 either replicating the boundary conditions of testing undertaken in this paper (to simulate a  
465 concrete façade) or with structural restraint conditions and applied loading to the samples  
466 to replicate likely behaviour in service, such as a concrete wall.

467 Scanning electron microscopy was performed to investigate the porosity of the cast  
468 samples. The image analysis performed supports the prior results from Orr et al. (2013),  
469 concluding that the studied fabric formed surface layer featured considerably lower  
470 porosity (over four times less porous) than the given timber formed layer.

471 With evidence showing the porosity of permeable mould formed surfaces to be lower (and  
472 thus, reducing the permeability of the surface, identified as a spalling hazard), it is  
473 recommended that further research be conducted on this topic.

## 474 **9 Further research**

475 Determining the effect on spalling of permeable moulds requires additional research. The  
476 non-spalling results found in this paper should not be extrapolated beyond the specific  
477 boundary conditions of the samples tested.

478 Fabrics with a range of pore sizes should be investigated, as the permeability of the mould  
479 is linked to the permeability of the cast concrete by the curing process.

480 Further testing to the same incident heat flux – time thermal exposures is recommended,  
481 on specimens with restrained end conditions to prevent bowing, and an applied  
482 compression load, to more realistically represent in-service fabric formed concrete.  
483 Determining the fire performance of permeably cast concrete remains an important  
484 research question to answer.

## 485 **10 Acknowledgments**

486 The authors wish to acknowledge the Building Research Establishment Centre for Fire  
487 Safety Engineering (University of Edinburgh), Microscopy and Analysis Suite (University of  
488 Bath) and laboratory staff from the Department of Architecture and Civil Engineering  
489 (University of Bath). CEMEX are gratefully acknowledged for providing mix design  
490 guidance and silica fume.

## 491 **11 Data access statement**

492 All data created in this paper are openly available from the data archive at  
493 <http://doi.org/10.10125/CAM> (TBC).

## 494 **12 References**

- 495 ASTM 2016. E119. *Standard Test Methods for Fire Tests of Building Construction and*  
496 *Materials*. West Conshohocken, PA: ASTM International.
- 497 BSI 2004. BS EN 1992-1-2. *Eurocode 2: Design of Concrete Structures - Part 1-2: General*  
498 *Rules - Structural Fire Design*. London: BSI.
- 499 BSI 2009a. BS EN 12390-3. *Testing hardened concrete. Part 3: Compressive strength of*  
500 *test specimens*. London, UK: BSI.
- 501 BSI 2009b. BS EN 13670. *Execution of concrete structures*. London: BSI.
- 502 CARRÉ, H., PIMIENTA, P., LA BORDERIE, C., PEREIRA, F. & MINDEGUIA, J. C. 2013.  
503 Effect of compressive loading on the risk of spalling. *MATEC Web of Conferences*.
- 504 CHANDLER, A. & PEDRESCHI, R. 2007. *Fabric Formwork*, London, RIBA.
- 505 FERREIRA, T. & RASBAND, W. 2011. *ImageJ User Guide*, Maryland, National Institutes  
506 of Health.
- 507 FRANK 2015. Zemdrain Controlled permeability formliner. Leiblfing Germany: DuPont.
- 508 GROSSHANDLER, W. 2002. NISTIR 6890 – Fire Resistance Determination and  
509 Performance Prediction Research Needs Workshop. Gaithersburg: National  
510 Institute of Standards and Technology.

511 HARMATHY, T. Z. 1965. Effect of moisture on the fire endurance of building materials.  
512 *ASTM Special Technical Publication, Moisture in Materials in Relation to Fire Tests*,  
513 74-95.

514 HAWKINS, W. J., HERRMANN, M., IBELL, P. T., KROMOSER, B., MICHAELSKI, A.,  
515 ORR, J. J., PRONK, A., SCHIPPER, R., SHEPHERD, P., VEENENDAAL, D.,  
516 WANSDRONK, R. & WEST, M. 2016. A state of the art review of flexible formwork  
517 technologies. *Structural Concrete*.

518 HERTZ, K. D. 2003. Limits of spalling of fire-exposed concrete. *Fire Safety Journal*, 38,  
519 103–116.

520 HERTZ, K. D. & SØRENSEN, L. S. 2004. Test method for Spalling of Fire Exposed  
521 Concrete. *Fire Safety Journal*, 40, 466-476.

522 HULIN, T., MALUK, C., BISBY, L., HODICKY, K., SCHMIDT, J. W. & STANG, H. 2015.  
523 Experimental studies on the fire behaviour of high performance concrete thin plates.  
524 *Fire Technology*, 52.

525 ISO 2002. ISO 834-8. *Fire-resistance tests -- elements of building construction -- part 8:*  
526 *Specific requirements for non-loadbearing vertical separating elements*. ISO.

527 JANSSON, R. 2008. *Material properties related to fire spalling of concrete*. Licentiate  
528 thesis, LUND INSTITUTE OF TECHNOLOGY.

529 JANSSON, R. 2013. *Fire Spalling of Concrete*. Doctoral thesis, Sweden.

530 KHOURY, G. A. 2000. Effect of fire on concrete and concrete structures. *Progress in*  
531 *Structural Engineering and Materials*, 2, 429–447. .

532 KLINGSCH, E. W. H. 2014. *Explosive Spalling of Concrete in Fire*. PhD thesis, ETH  
533 Zurich.

534 KODUR, V. K. R. & PHAN, L. 2007. Critical factors governing the fire performance of high  
535 strength concrete systems. *Fire Safety Journal*, 42, 482–488.

536 LAWSON, J. R., PARKER, A. & DEAN, S. W. 2009. A history of fire testing: Past, present,  
537 and future. *Journal of ASTM International*, 6.

538 LURA, P. & TERRASI, G. P. 2014. Reduction of fire spalling in high-performance concrete  
539 by means of superabsorbent polymers and polypropylene fibers. *Cement and*  
540 *Concrete Composites*, 49, 36–42.

541 MALUK, C. & BISBY, L. 2012. 120 years of structural fire testing: Moving away from the  
542 status quo. . *2nd Fire Engineering Conference*.

543 MALUK, C., BISBY, L., KRAJCOVIC, M. & TORERO, J. L. 2016. A Heat-Transfer Rate  
544 Inducing System (H-TRIS) Test Method. *Fire Safety Journal*.

545 MALUK, C., BISBY, L., TERRASI, G., KRAJCOVIC, M. & TORERO, J. L. 2012. Novel Fire  
546 Testing Methodology: Why, how and what now? . *Proceedings of the Mini*  
547 *Symposium on Performance-based Fire Safety Engineering of Structures*.

548 MALUK, C., BISBY, L. & TERRASI, G. P. 2013. Effects of polypropylene fibre type on  
549 occurrence of heat-induced concrete spalling. *MATEC Web of Conferences*.

550 MINDEGUIA, J.-C., PIMIENTA, P., HAGER, I. & CARRÉ, H. 2011. INFLUENCE OF  
551 WATER CONTENT ON GAS PORE PRESSURE IN CONCRETES AT HIGH  
552 TEMPERATURE.

553 ORR, J. J., DARBY, A. P., IBELL, P. T. & EVERNDEN, M. 2013. Durability enhancements  
554 using fabric formwork. *Magazine of Concrete Research*, 65, 1236-1245.

555 ORR, J. J., DARBY, A. P., IBELL, T. J., EVERNDEN, M. C. & OTLET, M. 2011. Concrete  
556 structures using fabric formwork. *The Structural Engineer*, 89, 20-26.

557 PRICE, W. F. 2000. Controlled permeability formwork. London: Construction Industry  
558 Research and Information Association.

559 RICKARD, I., GERASIMOV, N., BISBY, L. & DEENY, S. 2017. Predictive testing for heat  
560 induced spalling of concrete tunnel linings - The potential influence of sustained  
561 mechanical loading. *In: BOSTROM, L. & JANSSON MCNAMEE, R. (eds.)*

- 562 *Proceedings from the 5th International Workshop on Concrete Spalling*. Boras,  
563 Sweden: RISE Research Institutes of Sweden.
- 564 VEENENDAAL, D., WEST, M. & BLOCK, P. 2011. History and overview of fabric  
565 formwork: using fabrics for concrete casting. *Structural Concrete*, 12, 164-177.
- 566 ZEIML, M., LEITHNER, D., LACKNER, R. & MANG, A. 2006. How do polypropylene fibers  
567 improve the spalling behavior of in-situ concrete? *Cement and Concrete Research*,  
568 36, 929-942.
- 569 ZHANG, H. & DAVIE, C. 2013. A numerical investigation of the influence of pore pressures  
570 and thermally induced stresses for spalling of concrete exposed to elevated  
571 temperatures. *Fire Safety Journal*, 59, 102-110.
- 572